

# A framework for the description of charge order, pseudo and superconducting gap, critical temperature and pairing interaction in cuprate superconductors

E. V. L. de Mello<sup>1</sup>

<sup>1</sup>*Instituto de Física, Universidade Federal Fluminense, 24210-346 Niterói, RJ, Brazil\**

A unified phenomenological description framework is proposed for the evaluation of some of the most important observables of the cuprate superconductors: the pseudogap (PG)  $\Delta_{PG}$ , the local superconducting amplitudes  $\Delta_{SC}(r_i)$ , the critical temperature  $T_c$  and charge ordering (CO) parameters. Recent detailed measurements of CO structures and CO wavelengths  $\lambda_{CO}$  are faithfully reproduced by solutions of a Cahn-Hilliard differential equation with a free energy potential  $V_{GL}$  that produces alternating small charge modulations. The charge oscillations induce atomic fluctuations that mediate the SC pair interaction proportional to the  $V_{GL}$  amplitude. The local SC amplitude and phase  $\theta_i$  are connected by Josephson coupling  $E_J(r_{ij})$  and the SC long-range order transition occurs when  $\langle E_J \rangle \sim k_B T_c$ . The calculated results of the wavelength  $\lambda_{CO}$ ,  $\Delta_{PG}$ ,  $\langle \Delta_{SC} \rangle$  and  $T_c$  calculations are in good agreement with a variety of experiments.

A great deal of effort has been devoted to the investigation of the different energy scales of high-temperature superconductors, their hole-doping dependence and, most importantly, their interconnections<sup>1</sup>. These might provide clues to the pairing strength and to the superconducting (SC) mechanism. Under this program, Raman scattering on compounds with distinct average values of  $p$  holes per Cu atoms<sup>2,3</sup> identified vibration modes along the nodal direction ( $B_{2g}$ ) with energy  $\Delta_c(p)$  that follows closely  $T_c(p)$  and a second vibration mode measured along the antinode ( $B_{1g}$ ), identified with  $\Delta_{PG}(p)$  because it correlates well with the PG temperature  $T^*(p)$ . Other experiments like specific heat<sup>4</sup>, angle-resolved photon emission (ARPES)<sup>5,6</sup>, scanning tunneling microscopy (STM)<sup>7,8</sup> and submicron Josephson junction tunneling<sup>9</sup> identified also  $\Delta_{PG}(p)$  but measured another gap function ( $\Delta_0(p)$ ) that increases slowly in the underdoped region. In the overdoped region,  $\Delta_0(p)$  stays close to the PG and decreases rapidly beyond  $p \sim 0.20$  holes/Cu or simply  $p \sim 0.20$ . The interconnections among these three energy scales and their roles in the phase diagram of cuprates is the purpose of this letter. The present approach is complementary to that of Ref. 1 which studied several theoretical microscopic models and techniques with a  $d$ -wave SC order parameter and with pair density wave (PDW) fields that lead to the concept of intertwined orders.

To reveal this connection is of fundamental importance to consider also the leading role of the ubiquitous spontaneous symmetry breaking or anomalous incommensurate charge-ordering (CO)<sup>1,10</sup>. In particular, it was verified that the CO wavelength is correlated with the distance between the Fermi arcs tips, establishing an intriguing connection between CO in real space and the PG in  $k$ -space on  $\text{Bi}_2\text{Sr}_{2-x}\text{La}_x\text{O}_{6+\delta}$  ( $\text{Bi2201}$ )<sup>11,12</sup>. Many other experiments measure some kind of instability near  $T^*(p)$ , for instance, polar Kerr effect<sup>13</sup> and optical polarization rotation<sup>14</sup>. On the other hand, inhomogeneous magnetic-field response to muon spin rotation ( $\mu$ -SR)<sup>15</sup>, STM<sup>16,17</sup> and measurements of charge density wave (CDW) or CO by x-ray or resonant x-ray scattering (REXS)<sup>10-12,18-26</sup> have maximum signals near  $p = 0.12$  and do not follow the increasing trend of  $T^*$  when  $p \rightarrow 0$ , probably because of the vanishing of the available charge. However, all these observations may be regarded as distinct manifestations of an intrinsic

mesoscopic electronic phase separation with onset transition temperature  $T_{PS}$  near  $T^*(p)$ <sup>27</sup>, and this is a pillar of our approach. We recall, for further reference, that some systems like  $\text{La}_{2-x}\text{Sr}_x\text{CuO}_4$  have their average doping level  $x$  equal to the charge level  $p$  or the average number of holes/Cu, while for others, these quantities are not equal but proportional.

Nanoscale electronic phase separations are predicted theoretically by many different microscopic models, mostly based on the Hubbard Hamiltonian, like for instance Refs. [1, 28–33]. These rigorous calculations are important to endorse the phenomenon of electronic phase separation on highly correlated systems like the cuprates, but they neither reproduce the small variations<sup>10</sup> of  $\lambda_{CO}(p)$  nor the very fine charge modulations  $\Delta p \approx 10^{-2-3}$ , like in  $\text{YBa}_2\text{Cu}_3\text{O}_{6+\delta}$  (Y123)<sup>34</sup>. Another important point is that charge density modulations are unambiguously present in the entire system at low temperature and even above  $T_c$  according to STM data<sup>7,11,16,17,35,36</sup> and not in puddles occupying a volume fraction. This last point appears to be in conflict with the finite CO correlation lengths<sup>19-21,24</sup> but it is because the very weak nature of these electronic modulations and their strong fluctuations<sup>11</sup>.

In recent years there was an enormous improvement in the precision of the CO wavelength  $\lambda_{CO}$  measurements specially by STM, x-ray and REXS<sup>10</sup>. The very fine variation of  $\lambda_{CO}$  on  $p$  revealed in these experiments suggests the use of the time-dependent nonlinear Cahn-Hilliard (CH) differential equation<sup>37</sup>. In this approach the different charge oscillations may be tuned slowly up to reproduce the measured  $\lambda_{CO}$  and other forms of alternating hole-rich and hole poor regions on 100% volume fraction<sup>38-42</sup>.

The method has also the great advantage to concomitantly provide the free energy that yields a connection between the SC interaction and the charge modulations. The starting point is the time-dependent phase separation order parameter associated with the local electronic density,  $u(\mathbf{r}, t) = (p(\mathbf{r}, t) - p)/p$ , where  $p(\mathbf{r}, t)$  is the local charge or hole density at a position  $\mathbf{r}$  in the plane. The CH equation is based on the Ginzburg-Landau (GL) free energy expansion in terms of the conserved order parameter  $u$ <sup>38-43</sup>:

$$f(u) = \frac{1}{2}\varepsilon|\nabla u|^2 + V_{GL}(u, T), \quad (1)$$

where  $\varepsilon$  is the parameter that controls the charge modulations

and  $V_{GL}(u, T) = -\alpha[T_{PS} - T]u^2/2 + B^2u^4/4 + \dots$  is a double-well potential that characterizes the rise of charge oscillations below  $T_{PS}$  that is near  $T^*(p)$ . In general the values of  $\alpha$  and  $B$  are equated to unity. This free energy in terms of the phase separation order parameter is much simpler than the Ginzburg-Landau-Wilson free energy in terms of SC and PDW fields<sup>1</sup> but it suitably reproduces the details of the CO structure of distinct compounds and their localization energy  $V_{GL}$ .

The CH equation can be written in the form of the following continuity equation for the local free energy current density  $\mathbf{J} = M\nabla(\delta f/\delta u)$ ,<sup>44</sup>

$$\begin{aligned} \frac{\partial u}{\partial t} &= -\nabla \cdot \mathbf{J} \\ &= -M\nabla^2[\varepsilon^2\nabla^2u - \alpha^2(T)u + B^2u^3], \end{aligned} \quad (2)$$

where  $M$  is the mobility or the charge transport coefficient that sets both the phase separation time scale and the contrast between the values of  $u$  for the two phases.

The equation is solved by a stable and fast finite difference scheme with free boundary conditions<sup>43</sup> yielding the phase separation conserved order parameter  $u(\mathbf{r}, t = n\delta t)$ , function of position  $\mathbf{r}$  and  $n$  simulation time step  $\delta t$ . The limiting cases are  $u(\mathbf{r}_i, t) \approx 0$  corresponding to homogeneous systems above the pseudogap temperature  $T^*$  or small charge variations like the observed charge density wave (CDW) and  $u(\mathbf{r}_i, t \rightarrow \infty) = \pm 1$ , corresponding to the extreme case (at low temperatures) of complete phase separation. The local charge density is derived from  $p(\mathbf{r}, t) = p \times (u(\mathbf{r}, t) + 1)$  and the later case (strong phase separation) applies to static stripes<sup>45,46</sup> while the former (weak phase separation) to very small  $\Delta p \approx 10^{-2-3}$  variations around  $p$ , like that measured in  $\text{YBa}_2\text{Cu}_3\text{O}_{6+\delta}$  (Y123)<sup>34</sup>. We believe that such weak charge modulation masked CDW for many years and it is probably the reason to the very few charge inhomogeneities observations in the overdoped regime<sup>25,47</sup>.

Figure 1(a) shows a typical CH simulation ( $\text{La}_{2-x}\text{Sr}_x\text{CuO}_4$  (LSCO) for  $p = 0.15$ ) with a checkerboard pattern of  $\lambda_{CO} \sim 4a_0$  where  $a_0$  is the lattice parameter, while Fig. 1(b) shows  $V_{GL}(u(\mathbf{r}))$  or just  $V_{GL}(\mathbf{r})$  map that originates this specific charge structure. We discussed already these simulations in detail<sup>41,42</sup> and *here we want to focus mainly on the SC interaction* promoted by  $V_{GL}(\mathbf{r})$  that has a double role: First, it generates non-uniform charge patterns like the checkerboard modulation displayed in Fig. 1(a) that affect the ionic electronic clouds. The small atomic oscillatory displacements are verified by several neutron and x-ray scattering experiments<sup>19,48</sup>. Second, the small amplitude rapidly varying  $\Delta p$  are transmitted to the atomic electronic clouds that transmit them back to the holes, generating a hole-hole lattice mediated interaction.

In Fig. 1(c) we plot  $V_{GL}(x)$  along the  $x$ -direction together with some localized holes represented by the black filled circles. The planar Cu atoms are represented schematically on the top of Fig. 1(c) by the filled blue circles slightly displaced to (from) the hole-rich (poor) domains. When the temperature decreases below  $T^*$  the  $V_{GL}(\mathbf{r})$  modulations increase as shown schematically in the inset of Fig. 1(b) favoring alternating charge domains like those of Fig. 1(a). These domains

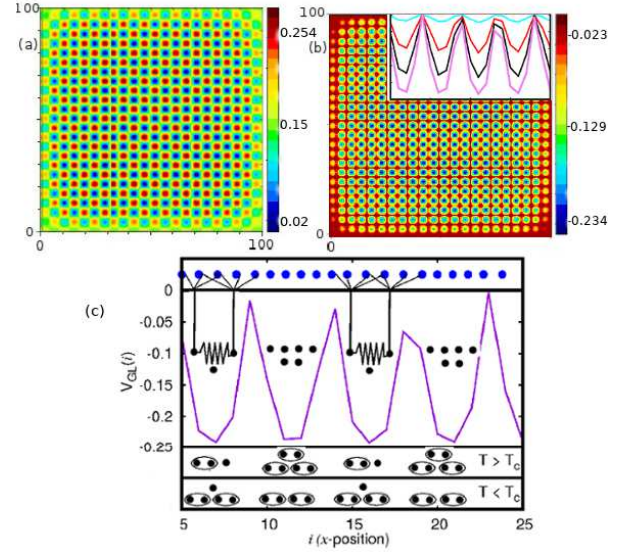


FIG. 1. (a) Low temperature simulation of a checkerboard charge density pattern for LSCO  $p = 0.15$  on 100 vs. 100 sites and (b) the  $V_{GL}(u(\mathbf{r}))$  that yields this density map. The inset shows how  $V_{GL}(x)$  evolves with the temperature below  $T^*$  or with the time of simulation  $\delta t$ . (c) The  $T = 0$  K limit of  $V_{GL}(x)$ . At the top, we represent some planar Cu atoms (blue filled circles) attracted to the hole-rich regions represented by straight lines as an illustration. Hole motion in the domains produces atomic fluctuations that affect other holes promoting an atomic mediated interaction that is represented by the springs for illustration. At  $T \leq T_c$  long-range order sets in, the Cooper pairs (the encircled pair of black dots) spread (superflowing) and the CO x-ray scattering signal decreases<sup>11,19</sup>.

are large compared with  $a_0$  and if the  $V_{GL}(\mathbf{r})$  modulations are high enough, the holes may move around or oscillate in the domains what induce also fluctuations on the nearby Cu atoms that, like a mirror, interact back with the other holes in the same domain.

This process leads to our main assumption; the SC local hole-hole pairing interaction is proportional to the spatial average  $\langle V_{GL}(p, 0) \rangle \equiv \sum_i^N V_{GL}(r_i, p, 0)/N$ , where the sum is over all the planar sites. The indirect role of the lattice in the SC interaction is confirmed by the relatively large isotope effect on the onset of superconductivity below  $T^*$  and also on  $T_c$ <sup>49</sup>.

With this phenomenological potential we developed a particular type of Bogoliubov-deGennes (BdG) SC approach that converges self-consistently to the local chemical potential  $\mu_i$  and the local  $d$ -wave amplitude  $\Delta_d(r_i)$ , keeping always the original CO structure fixed<sup>38-42</sup>. This is done diagonalizing the BdG matrix with the Hubbard Hamiltonian with hopping parameters taken from ARPES and nearest neighbor attractive potential with temperature dependence from the GL method;  $V_{GL}(p, T) = \langle V_{GL}(p, 0) \rangle [1 - T/T^*]^2$ .

Notice that  $V_{GL}(p, T)$  is defined as a function of the dimensionless phase separation order parameter  $u(\mathbf{r}, t)$  (Eq. 1) and needs to be multiplied by a dimensional constant to be converted to energy units in the Hubbard Hamiltonian. This

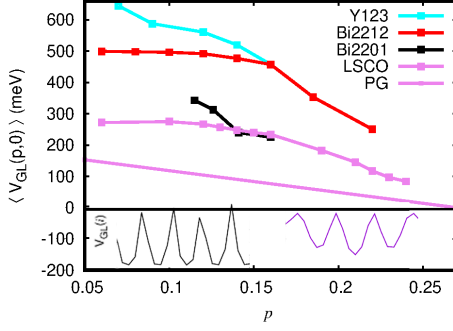


FIG. 2. The SC pair potential  $\langle V_{GL}(p,0) \rangle$  derived from the CO maps like that of Fig.1(b) converted in energy units (meV) to reproduce (with the BdG calculations) the SC gaps  $\Delta_0(p)$  in agreement with the experiments. We plot also the  $\Delta_{PG}(p)$  from Ref. [2] to illustrate its similar dependence on  $p$  with those of the averages  $\langle V_{GL}(p,0) \rangle$ . In the bottom, we show schematically the  $V_{GL}$  amplitude characteristic of the underdoped, respectively of the overdoped regions that are correlated with the SC interaction.

parameter is obtained making the low temperature CH-BdG calculations with the attractive potential  $\langle V_{GL}(p,0) \rangle$  in meV to yield the experimental optimal gap  $\langle \Delta_d(p_{opt} = 0.16, 0) \rangle$  also in meV. The very same constant is used to the other compounds potential  $\langle V_{GL}(p,0) \rangle$ , what gives only one adjustable parameter to all  $\langle \Delta_d(p, T) \rangle$  of a given family.

These CH-BdG calculations on a charge density map like that of Fig. 1(a) yield local SC amplitudes  $\Delta_d(r_i)$  inside each charge domain, in agreement with typical SC coherence length  $\xi_{SC}^{22,35,50}$  smaller<sup>51</sup> than typical  $\lambda_{CO}^{10}$ . The  $\Delta_d(r_i)$  plots have the same modulations of the charges, what is known as PDW, but in our approach this is a natural consequence of the simultaneous self-consistent approach on  $\mu_i$  and  $\Delta_d(r_i)^{42}$ . This is a different view of the proposal that PDW is a “parent” phase which spontaneously break symmetries and gives rise to the CDW and SC orders<sup>1</sup>.

To extend this approach to the overdoped region we recall our pillar connecting the CO with the PG and that  $T^*(p)$  vanishes only at  $p \approx 0.27$ , the end of the SC dome<sup>1,2,52</sup>. This argument suggests that weak incommensurate charge modulations are also present, most likely with much weaker amplitudes, in the overdoped region. In fact, different types of inhomogeneities are observed in overdoped Bi-based families<sup>8,16</sup> and in La-based materials<sup>5</sup> that is possibly connected with charge instabilities. Electronic transport anisotropy in the CuO plane that decreases with temperature and doping, persisting up to at least  $p \sim 0.22$  was recently measured and associated with a nematic phase<sup>25</sup>. More recently, REXS experiments in strong overdoped Bi2201 observed CO peak signals similar to those of underdoped cuprates<sup>47</sup>. They also measured a continued decrease of the CO vector  $Q_{CO}$  versus doping similar to what is seen in underdoped compounds<sup>10</sup>.

Taking these observations into consideration and the  $\lambda_{CO}(p)$  data of La and Bi-based compounds we extend the calculation to the overdoped region. The values of  $\langle V_{GL}(p,0) \rangle$  are plotted in Fig. 2 and used again in the BdG calculations to derive the low temperature SC gaps  $\langle \Delta_d(p, 0) \rangle$

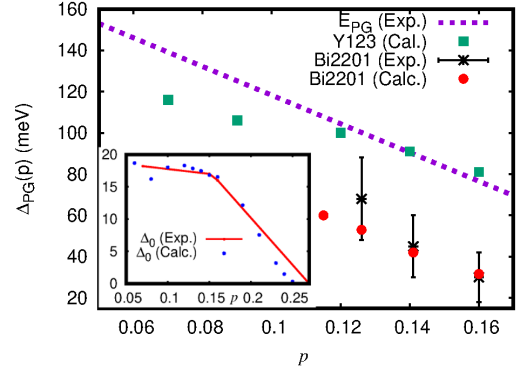


FIG. 3. The  $\Delta_{PG}$  of five Y123 and four Bi2201 calculated by Eq. 3 with experimental values of  $\lambda_{CO}$  compiled by Ref. [10] and the  $\langle V_{GL}(p,0) \rangle$  potential values from Fig. 2, without any adjusted parameter. The dashed line is an average of the experimental data from Ref. [2] and the Bi2201 experimental points and errorbars are from Ref. [11]. In the inset, the SC energy scale,  $\langle \Delta_0(p,0) \rangle$  from the BdG calculations with the  $\langle V_{GL}(p,0) \rangle$  potential of LSCO.

or  $\Delta_0(p)$  plotted in the inset of Fig. 3 for both under and overdoped  $\text{La}_{2-x}\text{Sr}_x\text{CuO}_4$  (LSCO). The results are close to the measured ARPES nodal gaps  $\Delta_0(p)$  extrapolated to the antinodal direction<sup>5,53</sup>, specific heat<sup>4</sup> and STM<sup>8</sup> measurements, indicating that  $\Delta_0(p)$  is a good candidate to the SC gap  $\Delta_{SC}(p)$ .

Now, we have the ingredients to demonstrate the correlation between the PG and the CO through the derivation of  $\Delta_{PG}(p)$  for Y123 and Bi2201 using the measured  $\lambda_{CO}(p)$  compiled in Ref.[10] and the  $\langle V_{GL}(p,0) \rangle$  that we derived and plotted in Fig. 2. We equate  $\Delta_{PG}(p,0)$  to the ground state energy of a shallow 2D well  $U = \langle V_{GL}(p,0) \rangle^{54}$ :

$$\Delta_{PG} = \frac{\hbar^2}{m\lambda_{CO}^2} \exp\left[-\frac{2\hbar^2}{m\lambda_{CO}^2 U}\right]. \quad (3)$$

The results of five Y123 and four Bi2201 calculations are plotted in Fig. 3 together with the experimental data<sup>2,11</sup>. The agreement near optimal doping is almost perfect and we emphasize that there is not any adjusted parameter in Eq. 3.

The agreement of the PG calculations endorses the CH-BdG calculations of CDW like structures with local SC order parameters inside the charge domains. In this scenario, the SC properties are similar to those of granular superconductors with Cooper pairs tunneling<sup>42</sup>. Such model was proposed earlier to explain the distribution of localized gaps detected by STM<sup>35</sup> and the SC correlations above  $T_c(p)$  in several materials<sup>50</sup>. In general, a SC order parameter has two components,  $(\Delta_d(r_i), \theta_i)$  what leads to the superconductivity in two steps and provides an explanations to the SC correlations measured at temperatures above  $T_c$ <sup>16,55-57</sup>. These experiments and our calculations of finite  $\Delta_d(r_i)$  and finite  $\langle \Delta_0(p, T) \rangle$  above  $T_c$  (shown, for instance, in Fig. 4(a) and (c)) suggest that the system resistance just above the SC transition comes from the persistent normal regions between the SC domains and their boundaries that oppose the Cooper pairs tunneling<sup>42</sup>.

In this case  $T_c(p)$  is the long-range phase order temperature obtained by Josephson coupling between the phases  $\theta_i$  in the



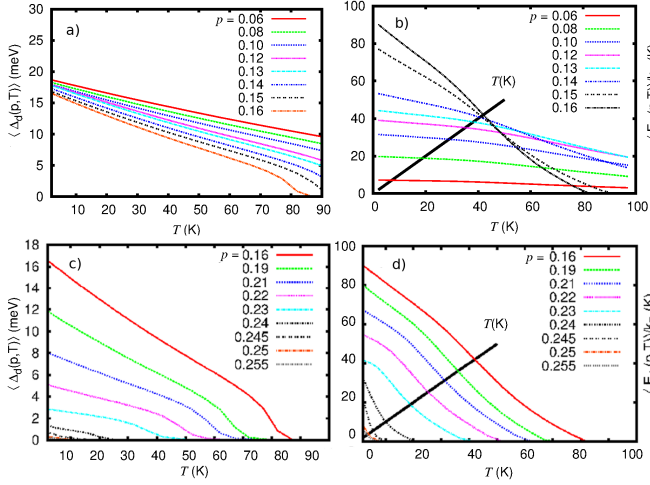


FIG. 4. a)  $\langle \Delta_d(p, T) \rangle$  for underdoped LSCO starting with the approximately constant  $\langle \Delta_0(p, 0) \rangle \approx 17.5 \text{ meV}$  that are close to the measured maximum gap  $\Delta_0(p)$  as shown in the inset of Fig. 3. b) Josephson energy  $\langle E_J(p, T) \rangle$  derived from the gaps shown in a). The intersections with  $k_B T$  yields the two sets of  $T_c(p)$ . c) The same of a) for overdoped LSCO compounds. d) Josephson energy  $\langle E_J(p, T) \rangle$  derived from the gaps shown in c).

charge domains. We have explained previously<sup>41</sup> that for a  $d$ -wave superconductor junction is sufficient to use the following  $s$ -wave analytical average Josephson coupling expression

$$\langle E_J(p, T) \rangle = \frac{\pi \hbar \langle \Delta_d(p, T) \rangle}{2e^2 R_n(p)} \tanh\left[\frac{\langle \Delta_d(p, T) \rangle}{2k_B T}\right], \quad (4)$$

where  $R_n(p)$  is taken to be proportional to the  $T \gtrsim T_c$  normal-state in-plane resistivity  $\rho_{ab}(p)$  obtained from typical  $\rho_{ab}(p, T)$  vs.  $T$  curves<sup>52</sup>. The proportionality constant between  $R_n$  and  $\rho_{ab}$  is found matching the optimal  $T_c \approx 42 \text{ K}$  for the case of LSCO. The other LSCO compounds use the same constant so that we need just a single adjustable parameter to derive  $T_c(p)$  for each cuprate system.

In Fig. 4(b) and (d) we plot  $\langle E_J(p, T) \rangle$  whose intersections with  $k_B T$ , represented by the black straight lines, yield  $T_c(p)$ . The results shown in Fig. 5 comprise all the CH-BdG calculations described previously in this paper yielding under and overdoped  $T_c(p)$  for the LSCO case. The agreement with the experiments is almost perfect, it deviates only in the strong overdoped region where the PG vanishes, the system become almost uniform and the  $\langle E_J(p, T) \rangle$  uncertainty is large. The  $T_c(p)$  dome shape has a simple interpretation with Eq. 4; the competing contribution of  $\langle \Delta_d(p, 0) \rangle$  that decreases steadily with  $p$  and vanishes near  $p = 0.27$  together with  $T^*(p)$  (see inset of Fig. 3), and  $R_n(p)$  that has an exponential decreasing behavior and diverges near  $p = 0.05$ . We should mention that other methods were also successful to reproduce the  $T_c(p)$  bell shape of cuprates, in particular, the method of Green function techniques with rigorous implementation of the non-standard commutation relations of the Hubbard operators<sup>28,29</sup>.

Another novel interpretation that comes out of this approach is that the Cooper pairs acquire long-range order at

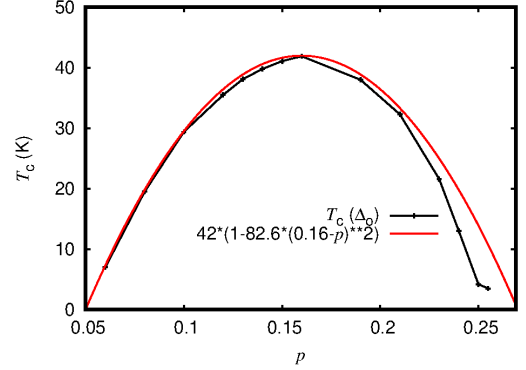


FIG. 5.  $T_c(p)$  calculation on the whole hole-doping region from the  $E_J$  of Eq. 4 and Figs. 4(b) (underdoped) and (d) (overdoped). The results reproduce the well-known LSCO measurements.

$T \sim T_c$  and like a superfluid spreads over the charge modulation domains on the CuO planes. This superflow uniforms the total charge density leading to a substantial decrease of the CO interference x-ray scattering signal. *This was interpreted as due to the competition between the CO and the SC phase*<sup>19,24</sup>, but it is a consequence of the local Cooper pairs long-range SC transition, as it is schematically shown at the bottom of Fig. 1(c) (for  $T > T_c$  and  $T < T_c$ ).

We have shown how to calculate the pseudogap  $\Delta_{PG}(p)$ , the average SC gap  $\langle \Delta_d(p) \rangle$  and  $T_c(p)$  of different cuprates in very good agreement with experiments from the measurements of  $\lambda_{CO}(p)$ . We remark that Ref. [1] proposes that the PDW order promotes other symmetry breaking phases of cuprates, in this context, we can say that our calculations show that the CDW order promotes the PG and SC  $d$ -wave phases. To deal with many important properties discussed in the paper and reproduce accurately several quantitative results, our approach is essentially phenomenological but should provide clear guidelines to any fundamental theoretical calculation on cuprates. Another advantage of our phenomenological theory is to reveal in a simple way the connection between the most fundamental energy scales and the relation between distinct properties like, for instance, the PG and the SC interaction.

The method is general and simple to be used in any problem involving superconductivity with CDW or any other type of charge instability that, otherwise do not have a simple theoretical approach. Under this program, we will soon present calculations on the correlation between the superfluid density  $\rho_{sc}(p, 0)$  and  $T_c(p)$ <sup>58</sup>, the interpretation of high magnetic field quantum oscillations experiments<sup>59</sup>, proximity effects, and other challenging problems of cuprates. Eq. 4 also points the way to combine materials to produce larger values of  $T_c$  what is important to technological applications.

I thank A. Bianconi, I. Božović, D. Möckli, J. Tranquada for helpful discussions and partial support by the Brazilian agencies CNPq and FAPERJ.

- 
- \* Corresponding author: evandro@if.uff.br
- <sup>1</sup> E. Fradkin, S. A. Kivelson, and J. M. Tranquada, *Rev. Mod. Phys.* **87**, 457 (2015).
  - <sup>2</sup> S. Huefner, M. A. Hossain, A. Damascelli, and G. A. Sawatzky, *Rep. Prog. Phys.* **71**, 062501 (2008).
  - <sup>3</sup> N. Munnikes *et al.*, *Phys. Rev. B* **84**, 144523 (2011).
  - <sup>4</sup> J. L. Tallon, J. W. Loram, J. R. Cooper, C. Panagopoulos, and C. Bernhard, *Phys. Rev. B* **68**, 180501 (2003).
  - <sup>5</sup> T. Yoshida, M. Hashimoto, I. M. Vishik, Z.-X. Shen, and A. Fujimori, *J. Phys. Soc. Japan* **81**, 011006 (2012).
  - <sup>6</sup> M. Hashimoto *et al.*, *Phys. Rev. B* **75**, 140503 (2007).
  - <sup>7</sup> T. Kato, T. Maruyama, S. Okitsu, and H. Sakata, *Journal of the Physical Society of Japan* **77**, 054710 (2008).
  - <sup>8</sup> J. W. Alldredge *et al.*, *Nature Physics* **4**, 319 EP (2008).
  - <sup>9</sup> J. K. Ren *et al.*, *Scientific Reports* **2**, 248 EP (2012).
  - <sup>10</sup> R. Comin and A. Damascelli, *Ann. Rev. of Cond. Mat. Phys.* **7**, 369 (2016).
  - <sup>11</sup> W. D. Wise *et al.*, *Nature Physics* **4**, 696 (2008).
  - <sup>12</sup> R. Comin *et al.*, *Science (New York, N.Y.)* **343**, 390 (2014).
  - <sup>13</sup> J. Xia *et al.*, *Phys. Rev. Lett.* **100**, 127002 (2008).
  - <sup>14</sup> Y. Lubashevsky, L. Pan, T. Kirzhner, G. Koren, and N. P. Armitage, *Phys. Rev. Lett.* **112**, 147001 (2014).
  - <sup>15</sup> Z. L. Mahyari *et al.*, *Phys. Rev. B* **88**, 144504 (2013).
  - <sup>16</sup> K. K. Gomes *et al.*, *Nature* **447**, 569 (2007).
  - <sup>17</sup> C. V. Parker, P. Aynajian, E. H. da Silva Neto, A. Pushp, S. Ono, J. Wen, Z. Xu, G. Gu, and A. Yazdani, *Nature* **468**, 677 (2010).
  - <sup>18</sup> T. Wu *et al.*, *Nature* **477**, 191 (2011).
  - <sup>19</sup> J. Chang *et al.*, *Nature Physics* **8**, 871 (2012).
  - <sup>20</sup> S. Blanco-Canosa *et al.*, *Physical Review B* **90**, 054513 (2014).
  - <sup>21</sup> M. Hückler *et al.*, *Physical Review B* **90**, 1 (2014).
  - <sup>22</sup> E. H. da Silva Neto *et al.*, *Science* **343**, 393 (2014), 1105.2508.
  - <sup>23</sup> G. Campi, *et al.*, *Nature* **525**, 359 (2015).
  - <sup>24</sup> R. Comin *et al.*, *Science (New York, N.Y.)* **347**, 1335 (2015).
  - <sup>25</sup> J. Wu, A. T. Bollinger, X. He, and I. Božović, *Nature* **547**, 432 (2017).
  - <sup>26</sup> W. Tabis *et al.*, *Phys. Rev. B* **96**, 134510 (2017).
  - <sup>27</sup> E. Fradkin and S. A. Kivelson, *Nature Physics* **8**, 864 (2012).
  - <sup>28</sup> N. M. Plakida, L. Anton, S. Adam, and G. Adam, *Journal of Experimental and Theoretical Physics* **97**, 331 (2003).
  - <sup>29</sup> N. M. Plakida and V. S. Oudovenko, *Journal of Superconductivity and Novel Magnetism* **29**, 1037 (2016).
  - <sup>30</sup> M. Vojta, *Phys. Rev. B* **66**, 104505 (2002).
  - <sup>31</sup> C. Ortix, J. Lorenzana, and C. Di Castro, *Phys. Rev. Lett.* **100**, 246402 (2008).
  - <sup>32</sup> L. Nie, A. V. Maharaj, E. Fradkin, and S. A. Kivelson, *Phys. Rev. B* **96**, 085142 (2017).
  - <sup>33</sup> S. Okamoto, D. Sénéchal, M. Civelli, and A.-M. S. Tremblay, *Phys. Rev. B* **82**, 180511 (2010).
  - <sup>34</sup> Y. A. Kharkov and O. P. Sushkov, *Scientific Reports* **6**, 34551 (2016).
  - <sup>35</sup> K. M. Lang *et al.*, *Nature* **415**, 412 (2002).
  - <sup>36</sup> T. Hanaguri *et al.*, *Nature* **430**, 1001 (2004).
  - <sup>37</sup> J. W. Cahn and J. E. Hilliard, *J. Chem. Phys.* **28**, 258 (1958).
  - <sup>38</sup> E. deMello, R. Kasal, and C. Passos, *J. Phys.: Condens. Matter* **21**, 235701 (2009).
  - <sup>39</sup> E. deMello, *Europhys. Lett.* **99**, 37003 (2012).
  - <sup>40</sup> E. deMello and R. Kasal, *Physica C: Superconductivity* **472**, 60 (2012).
  - <sup>41</sup> E. de Mello and J. Sonier, *J. Phys.: Condens. Matter* **26**, 492201 (2014).
  - <sup>42</sup> E. deMello and J. Sonier, *Phys. Rev. B* **95**, 184520 (2017).
  - <sup>43</sup> E. deMello and O. S. Filho, *Physica A* **347**, 429 (2005).
  - <sup>44</sup> A. Bray, *Adv. Phys.* **43**, 357 (1994).
  - <sup>45</sup> J. M. Tranquada, B. J. Sternlieb, J. D. Axe, Y. Nakamura, and S. Uchida, *Nature* **375**, 561 (1995).
  - <sup>46</sup> V. Thampy, X. M. Chen, Y. Cao, C. Mazzoli, A. M. Barbour, W. Hu, H. Miao, G. Fabbri, R. D. Zhong, G. D. Gu, J. M. Tranquada, I. K. Robinson, S. B. Wilkins, and M. P. M. Dean, *Phys. Rev. B* **95**, 241111 (2017).
  - <sup>47</sup> Y. Y. Peng *et al.*, *Nature Materials* **17**, 697 (2018).
  - <sup>48</sup> P. Abbamonte, *Phys. Rev. B* **74**, 195113 (2006).
  - <sup>49</sup> M. Bendele *et al.*, *Phys. Rev. B* **95**, 014514 (2017).
  - <sup>50</sup> Y. Imry, M. Strongin, and C. C. Homes, *Phys. Rev. Lett.* **109**, 067003 (2012).
  - <sup>51</sup> E. W. Carlson, V. J. Emery, S. A. Kivelson, and D. Orgad, *cond-mat.supr-con/0206217v1*.
  - <sup>52</sup> Y. Ando, S. Komiya, K. Segawa, S. Ono, and Y. Kurita, *Phys. Rev. Lett.* **93**, 267001 (2004).
  - <sup>53</sup> W. S. Lee *et al.*, *Nature* **450**, 81 (2007).
  - <sup>54</sup> L. Landau and E. Lifchitz, *Mécanique Quantique* (Éditions Mir, Moscow, Russie, 1966).
  - <sup>55</sup> A. Kanigel *et al.*, *Phys. Rev. Lett.* **101**, 137002 (2008).
  - <sup>56</sup> A. Dubroka *et al.*, *Phys. Rev. Lett.* **106**, 1 (2011).
  - <sup>57</sup> L. S. Bilbro, R. V. Aguilar, G. Logvenov, O. Pelleg, I. Božović, and N. P. Armitage, *Nature Physics* **7**, 298 (2011).
  - <sup>58</sup> E. deMello, (2020), arXiv:2001.07249.
  - <sup>59</sup> E. V. L. de Mello, *Journal of Physics: Condensed Matter* (2020).